nature structural & molecular biology

Conformational dynamics of ligand-dependent alternating access in LeuT

Kelli Kazmier[1,10], Shruti Sharma[2,10], Matthias Quick[3–5], Shahidul M Islam[6], Benoît Roux[6], Harel Weinstein[7,8], Jonathan A Javitch[3–5,9] & Hassane S Mchaourab[1,2]

The leucine transporter (LeuT) from *Aquifex aeolicus* is a bacterial homolog of neurotransmitter/sodium symporters (NSSs) that catalyze reuptake of neurotransmitters at the synapse. Crystal structures of wild-type and mutants of LeuT have been interpreted as conformational states in the coupled transport cycle. However, the mechanistic identities inferred from these structures have not been validated, and the ligand-dependent conformational equilibrium of LeuT has not been defined. Here, we used distance measurements between spin-label pairs to elucidate Na^+- and leucine-dependent conformational changes on the intracellular and extracellular sides of the transporter. The results identify structural motifs that underlie the isomerization of LeuT between outward-facing, inward-facing and occluded states. The conformational changes reported here present a dynamic picture of the alternating-access mechanism of LeuT and NSSs that is different from the inferences reached from currently available structural models.

NSSs include biogenic amine transporters that terminate synaptic signaling through selective reuptake of neurotransmitter molecules[1]. As targets of antidepressant molecules[2] and drugs of abuse[3], these transporters are critical in a spectrum of neuropsychiatric disorders[4,5] and in substance-addiction disorders[5]. LeuT is a bacterial Na^+-coupled amino acid transporter from *A. aeolicus* with broad specificity for small hydrophobic amino acids[6,7]. It has emerged as a paradigm for NSS transporters, owing to its sequence, structural and functional similarities that extend from highly conserved residues involved in ion and substrate coordination[6,8,9] to an overlapping spectrum of transport inhibitors[10]. LeuT is also the founding member of a fold class that encompasses sequence-unrelated symporters and antiporters. The conserved motif consists of an inverted repeat[11] of two sets of five transmembrane helices that coordinate the ions and substrates bound in a site near the middle of the membrane, and it is often stabilized by electrostatic interactions with unwound regions of transmembrane helices (TMs) 1 and 6 (ref. 6).

The current dogma of secondary active transport postulates 'alternating access' of the transporter that requires transition between at least two conformational states in which the ion- and substrate-binding sites are alternately exposed to the two sides of the membrane[12–15]. In this context, crystal structures of representative LeuT-fold transporters from multiple superfamilies have been classified as being in inward-facing, outward-facing or substrate-occluded states, cast as intermediates in the transport cycle, and then interpolated to describe plausible pathways of substrate binding and release[16–20]. A model of LeuT alternating access has emerged from crystal structures in three conformations (PDB 3TT1 (ref. 16), PDB 3TT3 (ref. 16) and PDB 2A65 (ref. 6) (**Fig. 1**)). Mutation of highly conserved residues and subsequent conformational selection by antibodies have been used to capture the inward- and outward-facing states[16]. However, the inference that the structures of these mutants represent actual intermediates in the alternating-access cycle has not been verified. Molecular dynamics (MD) simulations[21,22] and homology modeling[11] have elaborated on specific structural models of LeuT alternating access. A rocking-bundle model[11,23] envisioned conserved rearrangements between rigid scaffold and bundle domains in switching between outward- and inward-facing conformations. Steered MD simulations of LeuT uncovered a second substrate-binding site that was proposed to allosterically control the opening of an intracellular gate[21]. However, despite the wealth of structural data and extensive computational analyses, there is no consensus on the suite of conformational states that underlie alternating access in LeuT-fold transporters. A critical step toward this goal is the validation of the mechanistic identities of the available crystal structures and their incorporation into a dynamic framework of ion- and substrate-dependent equilibria[24–26].

Here, we used site-directed spin-labeling (SDSL)[27] and double electron-electron resonance (DEER) spectroscopy[28] to measure distance probabilities between spin-label pairs in LeuT in order to (i) define the ligand-dependent conformational equilibrium of LeuT,

[1]Chemical and Physical Biology Program, Vanderbilt University, Nashville, Tennessee, USA. [2]Department of Molecular Physiology and Biophysics, Nashville, Tennessee, USA. [3]Center for Molecular Recognition, Columbia University College of Physicians and Surgeons, New York, New York, USA. [4]Department of Psychiatry, Columbia University College of Physicians and Surgeons, New York, New York, USA. [5]New York State Psychiatric Institute, Division of Molecular Therapeutics, New York, New York, USA. [6]Department of Biochemistry and Molecular Biology, University of Chicago, Chicago, Illinois, USA. [7]Department of Physiology and Biophysics, Weill Medical College of Cornell University, New York, New York, USA. [8]HRH Prince Alwaleed Bin Talal Bin Abdulaziz Alsaud Institute for Computational Biomedicine, Weill Medical College of Cornell University, New York, New York, USA. [9]Department of Pharmacology, Columbia University College of Physicians and Surgeons, New York, New York, USA. [10]These authors contributed equally to this work. Correspondence should be addressed to H.S.M. (hassane.mchaourab@vanderbilt.edu).

Received 29 July 2013; accepted 27 March 2014; published online 20 April 2014; doi:10.1038/nsmb.2816

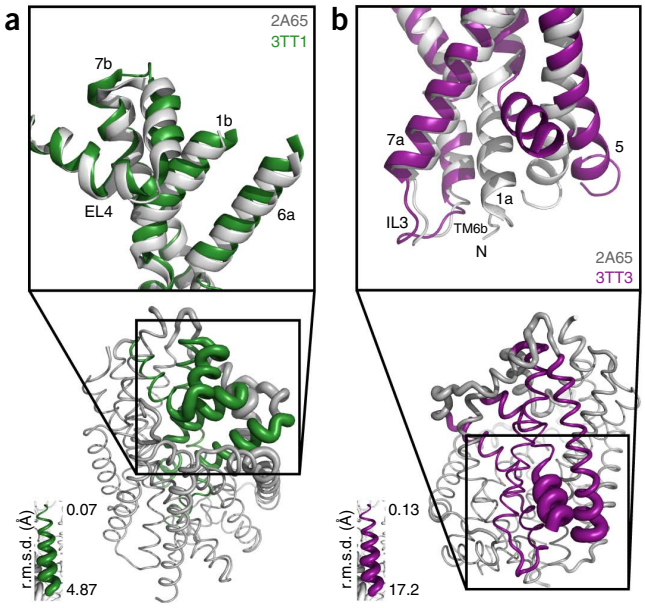

Figure 1 Model of LeuT alternating access inferred from the crystal structures. (**a**) r.m.s. deviations (r.m.s.d.) between occluded (PDB 2A65)[6] and outward-open (PDB 3TT1)[16] LeuT crystal structures mapped onto the outward-facing substrate-occluded structure. Inset, close-up view to highlight regions of most substantial differences: TMs 1 and 6, EL4 and TM7. (**b**) r.m.s. deviations between occluded (PDB 2A65) and inward-open (PDB 3TT3)[16] LeuT crystal structures mapped onto a ribbon diagram of the outward-facing substrate-occluded structure. The regions of most appreciable differences (TMs 1 and 5) as well as TMs 6 and 7 are shown in a close-up view.

(ii) identify the structural elements that mediate alternating access and (iii) investigate whether the LeuT conformational cycle involves isomerization between the structures identified in the crystal. From the interpretation of these results emerges a mechanism of LeuT alternating access that is at variance with the current picture inferred from the crystal structures[16].

RESULTS

To define the ligand-dependent equilibrium of LeuT between conformational states, we measured distance distributions between spin-label pairs under ligand conditions expected to promote transitions between transport intermediates[29,30]. We designed an extensive set of spin-label pairs to report a comprehensive view of the extracellular and intracellular sides of the transporter. On the extracellular side, we referenced distances to two sites in TMs 3 and 5 expected to be static. On the intracellular side, we selected reference sites in TMs 4 and 9.

We verified that all spin-labeled LeuT mutants introduced in the wild-type (WT) background bind leucine (**Supplementary Fig. 1**) in a Na^+-dependent manner. We observed changes in the level of binding relative to WT (**Supplementary Fig. 1a**) for mutants in TM6 as well as for spin-label pairs introduced in a Y268A background or an R5A background (**Supplementary Fig. 1a**). We constructed these two background mutations to mimic the disruption of an intracellular hydrogen-bonding network[29,31], as observed in the inward-facing LeuT crystal structure[6]. Analysis of binding isotherms demonstrates that the lower level of binding reflects lower affinity but similar substrate stoichiometry relative to the WT (**Supplementary Fig. 1b**). In addition, we measured Na^+-dependent alanine uptake in proteoliposomes for a large subset of mutants that are central to the interpretation of the results presented in this paper (**Supplementary Fig. 2a**,**b**). These data confirm that cysteine substitution and spin labeling do not impair the transport function of LeuT, in agreement with the findings from binding measurements.

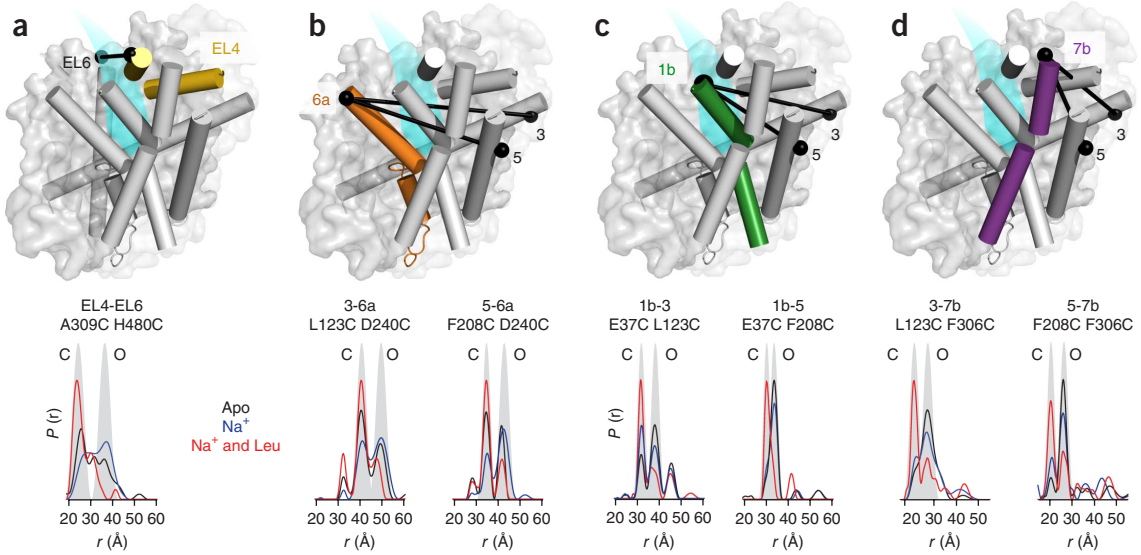

Figure 2 Na^+-induced opening and Na^+- and leucine-induced closing of the LeuT extracellular side. (**a**–**d**) Distance distributions depicting the probability of a distance $P(r)$ versus distance (r) between spin labels and reporting the conformational dynamics of EL4, TM6, TM1 and TM7 on the extracellular side of LeuT. The locations of representative spin-label pairs are highlighted on the substrate-occluded structure by black spheres connected by lines. TM helices expected to respond to ligand binding are shown as colored cylinders. The approximate location of the extracellular vestibule is colored cyan. Distance distributions for each pair were obtained in the apo, Na^+-bound (Na^+) and Na^+- and leucine-bound (Na^+ and Leu) intermediates. The multicomponent distributions reflect multiple conformations of LeuT in equilibrium. For illustration, we simulated the distance components corresponding to the outward-open (O) and outward-closed (C) conformations by using the average distance and width of each component. The resulting Gaussians are superimposed in gray. The shift in the conformational equilibria of EL4, TM6a, TM1b and TM7b relative to static reference points are shown in **a**–**d**, respectively.

LeuT Na^+- and leucine-dependent conformational equilibrium

DEER distance distributions describe the distance probabilities between a pair of spin labels[27,28]. In addition to reporting the average distance, the width of these distance distributions reflects dynamic modes that modulate the distance between the two spin labels[24,32,33]. Conformational sampling at room temperature is manifested as static disorder in the solid-state conditions under which the DEER data are collected. Thus, the broad and multicomponent distance distributions between pairs of labeled residues on the extracellular side of LeuT (**Fig. 2a–d**) are consistent with fluctuations between multiple conformations at equilibrium. To facilitate the assignment of distance components, we used different ligand conditions to enhance the populations of transporters in particular conformations. In the presence of Na^+ and leucine (**Fig. 2**), the distribution would be expected to favor the state captured by the crystal structure of Na^+- and leucine-bound LeuT (PDB 2A65), classified as substrate occluded[6]. In the presence of Na^+ (**Fig. 2**), the transporter would be expected to favor an outward-facing conformation poised to bind substrate[21,30]. In the absence of ion and substrate (apo condition), LeuT is expected to sample inward-facing, outward-facing and occluded conformations.

Our analysis identified two structural motifs, one consisting of extracellular loop (EL) 4 and TM6a (**Fig. 2a**,**b**) and the other consisting of TMs 1b and 7b (**Fig. 2c**,**d**). The first motif responded to Na^+ binding by an 'outward opening' that increased the population of the longer component in the distance distributions relative to apo (**Fig. 2a**,**b**). This component represents conformations wherein TM6a moves away from reference points in TMs 3 and 5 while EL4 moves away from EL6. Notably, the second motif was relatively less sensitive to Na^+, thus suggesting that even under apo conditions it already favored an outward-open conformation (**Fig. 2c**,**d**). As previously reported[30], transition to an outward-open conformation involves movements of extracellular loops, including EL2, EL3 and EL4, and is accompanied by increased water accessibility in the permeation pathway that leads to the binding site. Thus, we conclude that the movement of the two motifs underlies the change in accessibility of this vestibule.

We found that leucine binding induced concurrent shifts in the distance distributions of TMs 1, 6 and 7 and EL4 to favor the component associated with the closed positions (**Fig. 2**). In this presumably substrate-occluded conformation, TMs 1b, 6a and 7b moved closer to reference points in TMs 3 and 5. We infer that this movement is responsible for the reported reduced water accessibility in the vestibule upon leucine binding[30]. For TMs 1b, 6a, 7b and EL4, the magnitude of changes in the average distance between components corresponding to the outward-facing and substrate-occluded conformations was consistently >5 Å larger than that predicted by comparison of crystal structures of the states defined as outward facing and substrate occluded (**Fig. 1a**) (described below).

Similar interrogation of the dynamics at the intracellular side with a network of spin-label pairs identified TMs 6b and 7a and the N-terminal segment as undergoing the most substantial Na^+- and leucine-dependent movements (**Fig. 3a–d**). TM7a distance distributions were distinctly bimodal in the apo conditions, reflecting the equilibrium between inward-open and inward-closed conformations (**Fig. 3b**). The distances between TM7a and reference points in TM4 and IL1 decreased with inward opening. Binding of Na^+ or Na^+ and leucine shifted the equilibria in the same direction, i.e., both conditions favored the same distance component, consistently with stabilization of an inward-closed conformation (**Fig. 3b**). The nature of the TM6b movement was more challenging to define because its buried environment hindered spin-label incorporation at nondestabilizing, exposed sites (**Supplementary Figs. 1–3**). Nevertheless, spin-label pairs monitoring distances between the C-terminal loop of TM6 (intracellular loop (IL) 3) and TM4 showed ligand-dependent changes

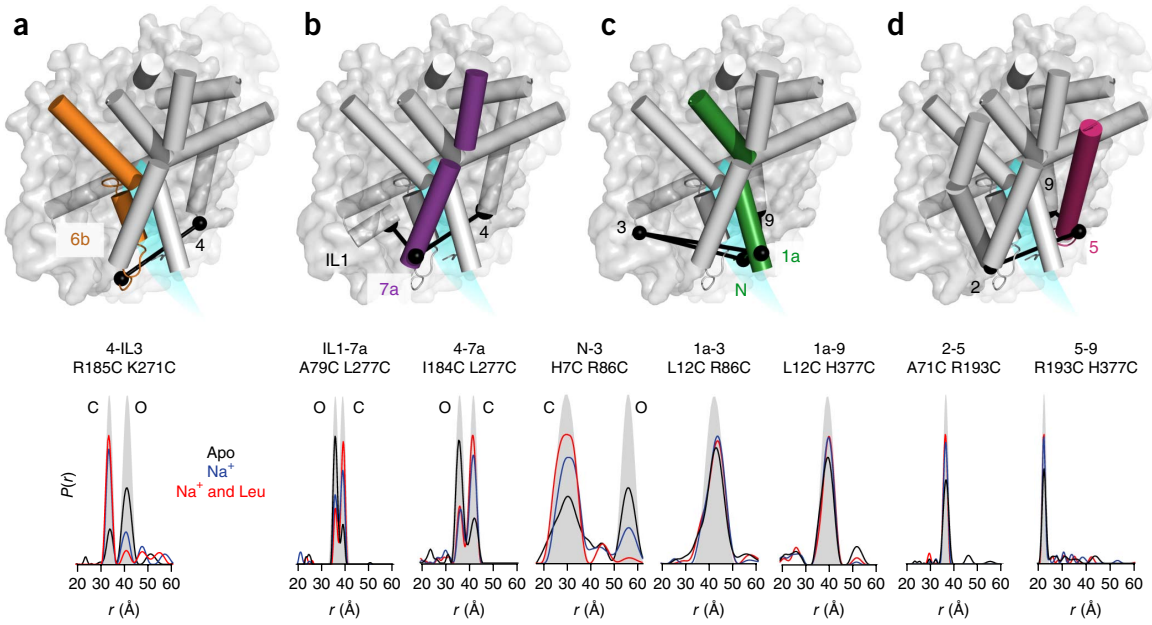

Figure 3 Fluctuation dynamics of TMs 6 and 7 and the N-terminal segment mediate the opening of the intracellular side of LeuT. (**a**–**d**) Distance distributions depicting the probability of a distance $P(r)$ versus distance (r) between spin labels and reporting the conformational dynamics of IL3, TM7, TM1 and TM5 on the intracellular side of LeuT. Distance distributions for each pair were obtained under three conditions as in **Figure 2**. Here, the simulated gray distributions reflect inward-open (O) and inward-closed (C) conformations. (**a**,**b**) IL3 and TM7a distributions, indicating an equilibrium between two conformations that is modulated by Na^+ and substrate binding. (**c**,**d**) Distributions for TMs 1a and 5, showing no ligand-dependent conformational changes.

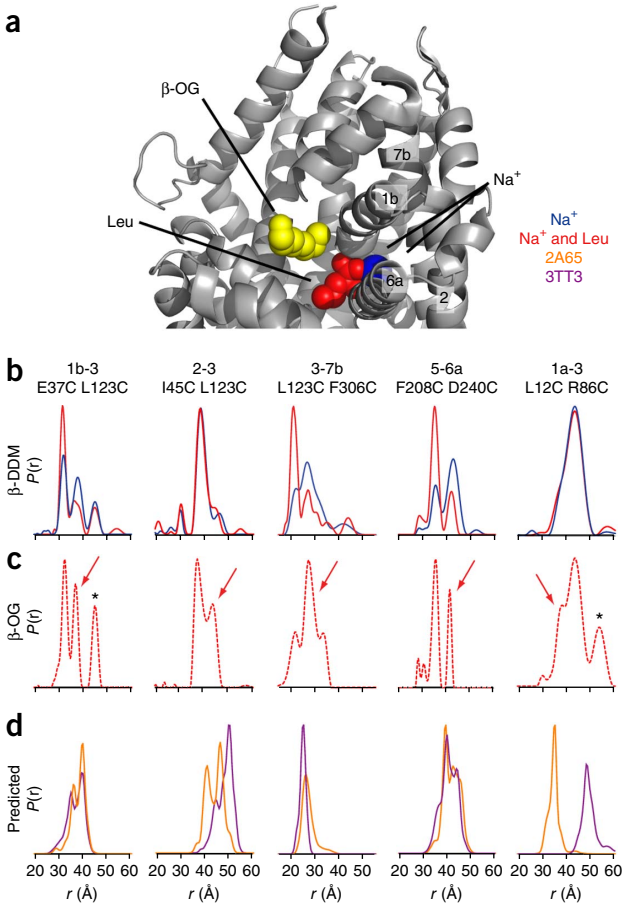

Figure 4 β-OG stabilizes the outward-facing conformation of LeuT in the presence of Na^+ and leucine. (**a**) Close-up view of the LeuT extracellular vestibule showing the simultaneous binding of leucine (red), Na^+ (blue) and β-OG (yellow) (PDB 3GJD[36]). Comparison of distance distributions in β-DDM (**b**) and β-OG (**c**), showing stabilization by β-OG of an outward-facing conformation on the extracellular side and a closed conformation on the intracellular side (TM1a and 3). The corresponding distance component is indicated by an arrow. The component labeled with an asterisk arises from aggregated protein during the concentration process. (**d**) Predicted distance distributions from three LeuT crystal structures (PDB 3TT1, outward facing; PDB 2A65, substrate occluded; PDB 3TT3, inward facing) from MMM (Online Methods).

in average distance and distribution width (**Fig. 3a**). The N-terminal segment (residues 1–10) displayed a Na^+- and leucine-dependent shift between two populations that represents the inward-open (longer distance component) and inward-closed positions (shorter distance component) (**Fig. 3c**). Presumably, this movement is associated with the release of a putative intracellular gate consisting of a network of charge interactions involving the N terminus and IL1 and stabilized by Tyr268 in IL3 (ref. 31) (**Supplementary Fig. 3a**).

Distance changes identify new LeuT conformational changes

On the basis of the inward-facing crystal structure[16], a large displacement of TM1a away from TM3 and TM9 that lifts TM1a upward toward the middle of the membrane is expected, along with a sizeable translation of TM5 relative to a scaffold of helices (**Fig. 1b**). Surprisingly, TM1a distance distributions measured here did not show components that would correspond to such a large amplitude movement (**Fig. 3c**), although changes in distribution widths indicated small-scale adjustments of TM1's position relative to TMs 3 and 9. Furthermore, TM5 distributions were consistently narrow, and the relative distance to other helices did not change as a result of binding of Na^+ or Na^+ and leucine (**Fig. 3d**).

To characterize and quantify the discrepancies between our DEER results and the inferences based on the crystal structures, we compared the distance distributions measured here with the distance distributions expected in the various crystal structures, the latter determined with the benchmarked spin-label rotamer library MMM[34,35] (**Supplementary Figs. 4** and **5**). On the extracellular side, a pattern of inconsistencies emerged in the distributions between TMs 1 or 6, and TMs 3 and 5 (**Supplementary Fig. 4**). Specifically, the distance component assigned to the occluded conformation (i.e., that favored by Na^+ and leucine, **Fig. 2b**,**c**) was consistently shorter than any component in the predicted distributions based on the PDB 2A65 structure (**Supplementary Fig. 4**). Thus, we infer that this crystal structure underestimates the closing of TMs 1b and 6a induced by binding of Na^+ and leucine in solution. Furthermore, the predicted distributions between TM7 and TMs 3 and 5 in the crystal structures of outward-open[16] and substrate-occluded[6] states (**Fig. 1a**) are superimposable, and this is inconsistent with the prominent movement of TM7b implied by the change in the distance distribution that we observed in the presence of Na^+ and leucine (**Fig. 2d**). Finally, although comparison of these crystal structures suggests movements of TM2 relative to TMs 3 and 5, we observed a tight distribution for these distances that was similar in the apo, Na^+-bound, and Na^+- and leucine-bound conditions (**Supplementary Fig. 4**).

β-OG may select for an outward-facing conformation

We reasoned that β-octyl glucoside (β-OG), the detergent used in most crystallization conditions[6,16] might be responsible for the discrepancies between our measurements of extracellular occlusion and those predicted by the crystal structures (**Fig. 4a–d**). Indeed, we found that exchange of LeuT from β-dodecyl maltoside (β-DDM) into β-OG shifts the experimental distance distributions for TMs 1, 2, 6 and 7 (**Fig. 4b**) toward the distance component assigned to the outward-open conformation (**Fig. 4c**), thereby partly or fully resolving the quantitative discrepancy with predicted distributions (**Fig. 4d**). This is consistent with the notion that a more outward-open conformation is favored in β-OG even in the presence of Na^+ and leucine, presumably as a result of the binding of a β-OG molecule in the extracellular vestibule (**Fig. 4a**)[36]. Together, these findings are consistent with PDB 2A65 representing an outward-facing state and not the occluded configuration that we observe in solution and that is expected upon binding of Na^+ and leucine.

On the intracellular side, the components in the distance distributions corresponding to the Na^+- and leucine-bound state for TMs 1 and 2 tended to be larger than those predicted from the substrate-occluded structure (PDB 2A65)[6] (**Supplementary Fig. 5**). The direction of the deviation and the effects of Na^+ and leucine suggest that TM1 favors a more open conformation relative to that observed in the outward-facing[16] or substrate-bound[6] crystal structures. In contrast to the extracellular side, the shift in the distance distributions upon exchange into β-OG favored the shorter distance component (**Fig. 4b**,**c**), which overlapped with the distribution predicted on the basis of the occluded crystal structure determined in the presence of Na^+ and leucine (**Fig. 4d**). Thus the LeuT conformation in β-OG is more outward open and inward closed, both in the PDB 2A65 structure and in our DEER measurements. This suggests that the actual substrate-occluded state (in the absence of β-OG) is more closed at

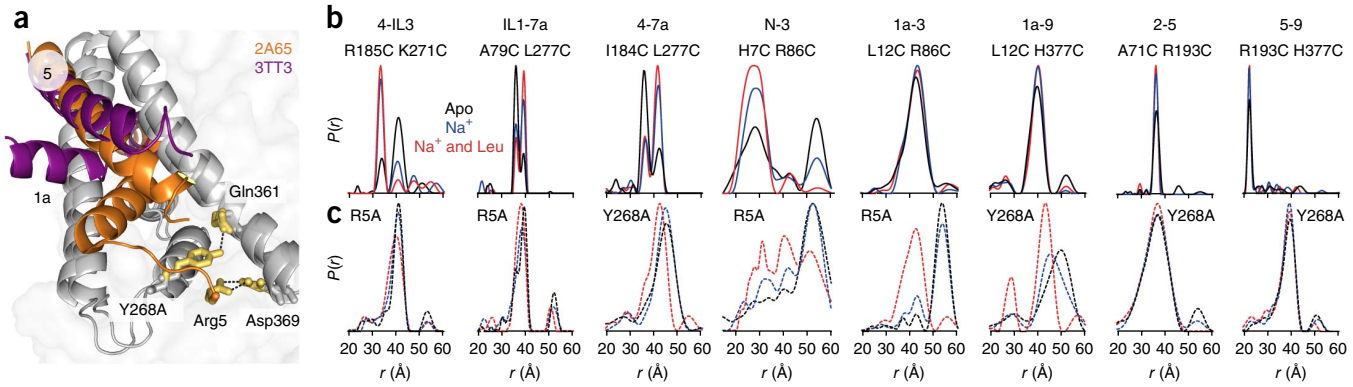

Figure 5 The Y268A or R5A mutations induce structural rearrangements in LeuT. (**a**) Close-up view of the putative intracellular gate showing the network of charge interactions stabilized by Tyr268 and involving Arg5. TMs 1 and 5 are highlighted. (**b**,**c**) Distance distributions from **Figure 3** in WT (**b**) and the intracellular-gate mutant background (**c**). Dashed lines in **c** indicate the appearance of new distance components in the distributions of TMs 1 and 5 in the Y268A and R5A mutants that are not present in the WT background (**b**) under apo conditions.

the extracellular side and more open at the intracellular side than the PDB 2A65 structure is.

Y268A mutation uncouples helical movements from Na^+ and leucine binding

Crystallization of LeuT in the inward-open structure required multiple mutations to disrupt the intracellular gate and to weaken the second Na^+-binding site (Na2)[16]. The former was achieved through the substitution of a highly conserved tyrosine (Tyr268) in TM6b with an alanine. Therefore, we monitored the distance distributions of TM1a and TM5 on the intracellular side in a Y268A background (**Fig. 5a**–**c**). Compared to distance distributions in the WT background (**Fig. 5b**), the pattern of distance changes in this mutant background (**Fig. 5c**) recapitulated many aspects of the inward-facing[16] crystal structure (**Fig. 5a**). TM1a underwent a 15-Å change in distance relative to TM9 (**Fig. 5c**), which lifted TM1a toward the middle of the membrane, thus leading to a short distance component relative to the extracellular side of TM8 (**Supplementary Fig. 6**). The marked displacement of TM5 deduced from the inward-facing crystal structure (**Fig. 5a**) was also captured by the distance distribution to TM9 (**Fig. 5b**,**c**). However, this 'opening' movement of TM5 was not reversed by the presence of Na^+ and leucine (**Fig. 5c**), despite direct biochemical evidence that these mutants bind leucine, albeit with lower affinity (**Supplementary Figs. 1** and **2**). Thus, in the mutant background, TM5 did not reset to its closed position even in the presence of Na^+ and leucine. Another mutation that has been shown to disrupt the intracellular gate, R5A (**Fig. 5a** and **Supplementary Fig. 3a**)[29,31], yielded distance changes similar to those in Y268A (**Fig. 5c**). Thus, the mutations used to generate the inward-open[16] crystal structure shift a major population of the transporters to a conformation that is not readily observed in the ensemble of states sampled in the WT background.

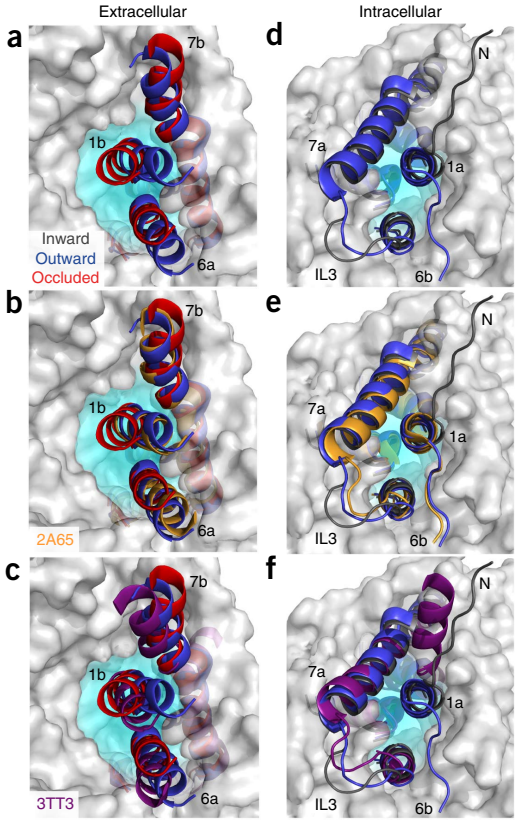

Figure 6 Models of LeuT conformational changes derived from restrained ensemble simulations. (**a**–**c**) Extracellular view of the occluded (red) and outward-facing (blue) models of LeuT (**a**), derived from the DEER restraints, superimposed on the substrate-occluded crystal structure (PDB 2A65, orange) (**b**) and the inward-facing crystal structure (PDB 3TT3, purple) (**c**). Prominent displacements of TMs 1a and 6b (red model) to close the extracellular vestibule are present in the occluded conformation relative to the crystal structures. (**d**–**f**) Intracellular view of the inward-facing model (black), derived from the DEER restraints, superimposed on the outward-facing model (blue) (**d**), the substrate-occluded structure (PDB 2A65, orange) (**e**) and the inward-facing structure (PDB 3TT3, purple) (**f**).

Restrained ensemble modeling of LeuT conformational changes

To describe the coordinated structural changes induced by binding of Na^+ and leucine, we carried out MD simulations restrained by the DEER distance distributions by using the recently described restrained ensemble (RE) method[37,38]. We inserted multiple copies of 'dummy' spin labels, previously parameterized from all-atom simulations of the spin label, at sites for which the DEER distance-distribution data are available (**Fig. 6a**–**f**) and allowed the transporter backbone to adjust dynamically to match the experimental distributions. The experimental distance distributions were effectively imposed on the multiple copies of the dummy spin labels via a large harmonic potential

(Online Methods). For all the simulations, the substrate-occluded crystal structure (PDB 2A65) was used as the starting conformation. TMs 2–5, 8 and 9 were held fixed on the basis of distance distributions that did not change in response to ligand binding (**Supplementary Fig. 7**). We found that imposing the DEER restraints corresponding to the Na^+-bound state did not lead to substantial changes in the LeuT structure, in agreement with our finding that it represents an outward-facing conformation (**Fig. 6a–c**). In contrast, we observed substantial changes in the backbone when the structure was refined with DEER restraints from the Na^+- and leucine-bound state, with notable shifts of extracellular TMs 1 and 6 toward the vestibule, as expected from a closing motion (**Fig. 6a–c**). The movement of extracellular TM7 was in a different direction, but we suggest that this motion enabled the capping of the vestibule by EL4 (ref. 30). Similarly, we found that imposing the EPR restraints representing the inward-facing conformation drove backbone changes in the N terminus and TMs 1 and 7 on the intracellular side (**Fig. 6d–f**). However, the amplitudes of these changes were smaller than those demonstrated experimentally in the distance distributions. In this case, the backbone displacements have been largely obscured by excessive rotameric sampling of the dummy label, which was previously optimized to best match DEER data for solvent-exposed sites in T4 lysozyme but which might be overestimated in the present situation[37,38]. This effect was also present on the extracellular side, limiting the magnitude of evident conformational changes, but to a lesser degree. A contributing factor to this discrepancy may have been the sparsity of restraints on the intracellular side, which were limited by design as a consequence of tight packing of secondary structures. Overall, the RE simulations confirm that the Na^+-bound and Na^+- and leucine-bound crystal structures represent outward-facing structures, demonstrate that the inward-facing crystal structure is incompatible with the DEER data in the WT background and outline the structural elements involved in the transition to the occluded and inward-facing conformations, neither of which was observed previously[6,16].

DISCUSSION

Structural motifs underlying alternating access of LeuT

The pattern and ligand dependence of distance changes gleaned from the distributions and validated by the RE simulations identifies movements of motifs at the extracellular (1b and 7b, 6a and EL4) and intracellular ends (6b and 7a, N terminus) of LeuT (**Fig. 7**). In the absence of ligands, both motifs can sample open and closed positions, thus enabling apo-LeuT to isomerize between conformations, as would be expected for a symporter (**Fig. 7a**,**f**), although the equilibrium favors the inward-facing conformation. Binding of Na^+, which engages the unwound segments of TMs 1 and 6, concomitantly shifts the equilibria of the extracellular and intracellular motifs, effectively favoring an outward-open and inward-closed conformation of LeuT (**Fig. 7b**). Substrate, which is primarily coordinated by the unwound regions of TMs 1 and 6 in the primary binding site (S1), resets these two TMs to their closed positions (**Fig. 7c**). Together, these observations suggest that the rearrangements of the intracellular and extracellular motifs reported here are mechanistically important for the alternating-access mechanism in LeuT.

One of the major findings of this work is that the ligand-dependent coupling of the extracellular side of the transporter with its intracellular side involves both TMs 6 and 7. Although TM6 was proposed to be a pivotal element in the isomerization of LeuT, on the basis of its direct contact with ligands, the ion- and substrate-dependent movement of TM7 described here is new. The coupled but opposite shifts in the equilibria of the extracellular part of TM6 (TM6a) and the intracellular part of TM7 (TM7a) ensure that the intracellular motif and the extracellular motifs are not concurrently open. We suggest that the movement of TM7 was obscured in the crystal structures by the tendency to trap LeuT in outward-facing conformations, possibly by the binding of β-OG in the extracellular vestibule[6,16].

The proposed movement of the intracellular and extracellular motifs are grounded in aspects of TM flexibility that have been inferred from the crystal structures[6,16]. Specifically, the pivot points observed crystallographically in TMs 1, 6 and 7 rationalize the hinge-like bending of

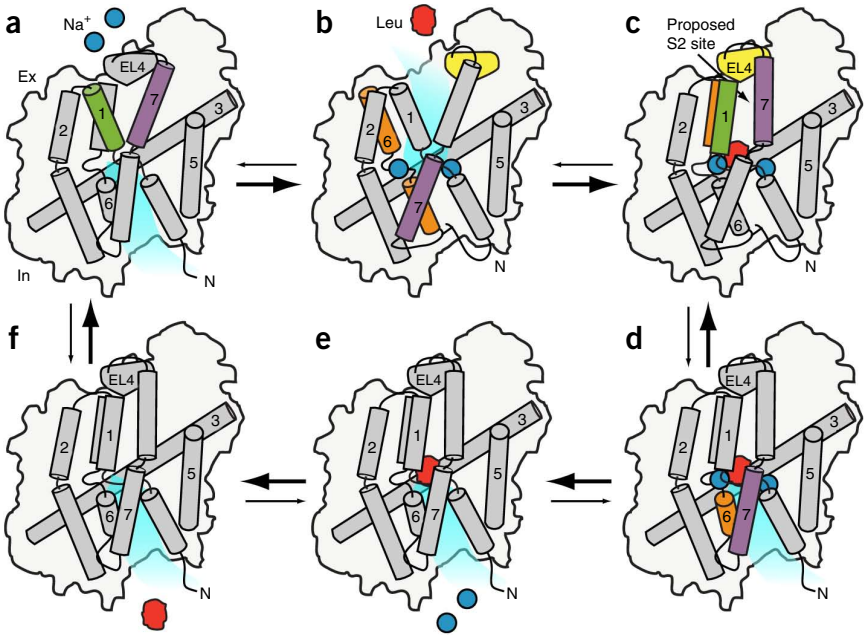

Figure 7 Cartoon model of LeuT transport derived from EPR data. Transmembrane helices involved in conformational changes at each step in the transport cycle are highlighted in color. (**a**) The cycle begins after release of ion and substrate to the intracellular side (In). Apo-LeuT samples inward-facing (**a**) and outward-facing conformations (**b**). (**b**) Na^+ binding favors opening of the extracellular side (Ex) through shifts in the equilibria of the extracellular motifs. Coupled closing of the intracellular side involves a shift in the equilibrium of the intracellular motif to its closed position, to stabilize the intracellular gate. (**c**) Leucine binding at the S1 site, and potentially at a proposed S2 site, causes a large-scale closure of the extracellular side, thus leading to an occluded state. (**d**) Fluctuations on the intracellular side, facilitated by the unwound region of TM6 and a kink at Gly294 of TM7, mediate the opening of the intracellular side. (**e**) Na^+ dissociates to the intracellular solution, where its concentration is low. (**f**) In the absence of bound Na^+, leucine affinity to LeuT is reduced, thus driving its dissociation to the intracellular side. The cycle continues through the isomerization from inward-facing (**f**) to outward-facing (**a**).

these TMs required for the transition between inward-facing and outward-facing states in our model (**Fig. 7**). Although TM7 does not have an unwound region, a hinge-like bend at Gly294 was evident in the inward-facing crystal structure. Small ion- and substrate-dependent movements are noted for TMs 1, 10 and 11 on the intracellular side; the latter two most probably serve to facilitate the movement of the intracellular motif that they cradle (**Supplementary Fig. 7b**). Importantly TM1a's more open position relative to the crystal structure (**Fig. 4**) is consistent with MD simulations[22] that invoke TM1a movement in facilitating substrate release. Notably, these simulations were initiated from the Na^+- and leucine-bound crystal structure, so that the dynamic nature of TM1a in the simulations may reflect both the relaxation to its position in the occluded conformation in the absence of β-OG and the response to the progress of substrate toward the intracellular release site. Indeed, the broad distributions of TM1a suggest that this helix is relatively dynamic, and with TM1a favoring a more open position relative to the PDB 2A65 structure, the movement of the intracellular motif (**Fig. 7d–f**) enables substrate exit on the intracellular side of the transporter. Krishnamurthy *et al.*[16] proposed that in the absence of bound Na^+ it is energetically unfavorable for TM1a to remain in a closed position. Although our data support a dynamic TM1a under apo conditions, the implication that it is favorable for TM1a to lift up into the membrane now seems unlikely, given the absence of large-amplitude, ion-dependent movement of this TM in the WT background.

Mechanism of transport

Coupled transport requires the binding of ions and substrates on one side of the membrane followed by conformational changes to enable subsequent ion and substrate dissociation at the other side of the membrane. Symported ions that power the uphill movement of substrates could stabilize and destabilize substrate binding in the outward- and inward-facing conformations, respectively, conferring directionality to the transport process by their concentration gradients. Additionally, ion binding could alter the energetics of the equilibrium in the ensemble of conformations, increasing the population of those conformations in which the substrate site is open to the extracellular milieu. In LeuT, Na^+ fulfills both roles: its binding biases the equilibrium to favor an outward-facing conformation, and it subsequently directly coordinates the substrate at the unwound regions of TMs 1 and 6.

We and others[29,30] have found that substrate binding induces occlusion of the binding site on both sides of the transporter (**Fig. 7c**). Thus, the energetically unfavorable release of leucine has to be facilitated by low-probability equilibrium fluctuations of the intracellular motif (TMs, 6, 7 and N terminus) to its open position (**Fig. 7d**). We surmise that these fluctuations must be coupled to the favorable movement of Na^+ down its concentration gradient. Previous studies[21,39] have proposed that the dissociation of Na^+ at the Na2 site (**Fig. 7e**) in the presence of substrate enhances inward opening and facilitates inward release of the Na^+ at the first Na^+-binding site (Na1). The loss of this Na^+ reduces the affinity of substrate, thus enhancing leucine dissociation to the cytoplasm (**Fig. 7f**).

The transport-cycle scheme presented in **Figure 7** departs from the rocking-bundle model[11,23] in fundamental aspects. The latter invokes rotation of the entire bundle relative to the scaffold to mediate the alternating access of the transporter. Although TMs 1, 6 and 7 are part of the bundle, they do not move as rigid bodies but flex around hinge points. Moreover, the extracellular and intracellular opening and closing are not mediated by the same helices. Notably TM2's movement does not substantially change its distance relative to the scaffold in response to ligand binding. Finally, the prominent movement of EL4 and the N-terminal region are not considered in the rocking-bundle model.

The new insight offered by the data presented here suggests a new set of conformational changes underlying alternating access by LeuT and sets the stage for further analysis to determine the transition path between these states. This is a critical step toward elucidating the mechanism of Na^+-coupled transport by LeuT and LeuT-fold transporters.

METHODS

Methods and any associated references are available in the online version of the paper.

Note: Any Supplementary Information and Source Data files are available in the online version of the paper.

ACKNOWLEDGMENTS

The authors gratefully acknowledge R. Stein for assistance with EPR data collection and EPR distance analysis. We thank H. Koteiche and P.R. Steed for critical reading and editing of the manuscript. We thank Extreme Science and Engineering Discovery Environment (XSEDE) for computer time. This work was supported by US National Institutes of Health grants U54-GM087519 (H.S.M., S.S., H.W., J.A.J., S.M.I. and B.R.), K05DA022414 (J.A.J.) and P01DA012408 (H.W.). K.K. was supported by a predoctoral National Research Service Award (F31-MH095383-01).

AUTHOR CONTRIBUTIONS

K.K. and S.S. constructed mutants, expressed and purified protein, prepared samples and conducted DEER experiments. K.K. and H.S.M. designed the DEER experiments. K.K., S.S. and H.S.M. analyzed DEER data and interpreted the distance distributions. M.Q. designed, conducted and analyzed leucine-binding and alanine-transport experiments. S.M.I. and B.R. refined structural models with the restrained ensemble simulations method. All authors contributed to the mechanistic interpretation of the data, wrote and edited the manuscript.

COMPETING FINANCIAL INTERESTS

The authors declare no competing financial interests.

1. Rudnick, G. in *Neurotransmitter Transporters* (ed. Reith, M.A.) 25–52 (Humana Press, 2002).
2. Iversen, L. Neurotransmitter transporters and their impact on the development of psychopharmacology. *Br. J. Pharmacol.* **147** (suppl. 1), S82–S88 (2006).
3. Amara, S.G. & Sonders, M.S. Neurotransmitter transporters as molecular targets for addictive drugs. *Drug Alcohol Depend.* **51**, 87–96 (1998).
4. Singh, S.K. & Leu, T. A prokaryotic stepping stone on the way to a eukaryotic neurotransmitter transporter structure. *Channels (Austin)* **2**, 380–389 (2008).
5. Gether, U., Andersen, P.H., Larsson, O.M. & Schousboe, A. Neurotransmitter transporters: molecular function of important drug targets. *Trends Pharmacol. Sci.* **27**, 375–383 (2006).
6. Yamashita, A., Singh, S.K., Kawate, T., Jin, Y. & Gouaux, E. Crystal structure of a bacterial homologue of Na^+/Cl^--dependent neurotransmitter transporters. *Nature* **437**, 215–223 (2005).
7. Singh, S.K., Piscitelli, C.L., Yamashita, A. & Gouaux, E. A competitive inhibitor traps LeuT in an open-to-out conformation. *Science* **322**, 1655–1661 (2008).
8. Beuming, T., Shi, L., Javitch, J.A. & Weinstein, H. A comprehensive structure-based alignment of prokaryotic and eukaryotic neurotransmitter/Na^+ symporters (NSS) aids in the use of the LeuT structure to probe NSS structure and function. *Mol. Pharmacol.* **70**, 1630–1642 (2006).
9. Kanner, B.I. & Zomot, E. Sodium-coupled neurotransmitter transporters. *Chem. Rev.* **108**, 1654–1668 (2008).
10. Kristensen, A.S. *et al.* SLC6 neurotransmitter transporters: structure, function, and regulation. *Pharmacol. Rev.* **63**, 585–640 (2011).
11. Forrest, L.R. *et al.* Mechanism for alternating access in neurotransmitter transporters. *Proc. Natl. Acad. Sci. USA* **105**, 10338–10343 (2008).
12. Mitchell, P. A general theory of membrane transport from studies of bacteria. *Nature* **180**, 134–136 (1957).
13. Jardetzky, O. Simple allosteric model for membrane pumps. *Nature* **211**, 969–970 (1966).
14. Vidaver, G.A. Inhibition of parallel flux and augmentation of counter flux shown by transport models not involving a mobile carrier. *J. Theor. Biol.* **10**, 301–306 (1966).

15. Patlak, C.S. Contributions to the theory of active transport: II. The gate type non-carrier mechanism and generalizations concerning tracer flow, efficiency, and measurement of energy expenditure. *Bull. Math. Biophys.* **19**, 209–235 (1957).
16. Krishnamurthy, H. & Gouaux, E. X-ray structures of LeuT in substrate-free outward-open and apo inward-open states. *Nature* **481**, 469–474 (2012).
17. Shimamura, T. *et al.* Molecular basis of alternating access membrane transport by the sodium-hydantoin transporter Mhp1. *Science* **328**, 470–473 (2010).
18. Watanabe, A. *et al.* The mechanism of sodium and substrate release from the binding pocket of vSGLT. *Nature* **468**, 988–991 (2010).
19. Perez, C., Koshy, C., Yildiz, O. & Ziegler, C. Alternating-access mechanism in conformationally asymmetric trimers of the betaine transporter BetP. *Nature* **490**, 126–130 (2012).
20. Shaffer, P.L., Goehring, A., Shankaranarayanan, A. & Gouaux, E. Structure and mechanism of a Na^+-independent amino acid transporter. *Science* **325**, 1010–1014 (2009).
21. Shi, L., Quick, M., Zhao, Y., Weinstein, H. & Javitch, J.A. The mechanism of a neurotransmitter:sodium symporter–inward release of Na^+ and substrate is triggered by substrate in a second binding site. *Mol. Cell* **30**, 667–677 (2008).
22. Shi, L. & Weinstein, H. Conformational rearrangements to the intracellular open states of the LeuT and ApcT transporters are modulated by common mechanisms. *Biophys. J.* **99**, L103–L105 (2010).
23. Forrest, L.R. & Rudnick, G. The rocking bundle: a mechanism for ion-coupled solute flux by symmetrical transporters. *Physiology (Bethesda)* **24**, 377–386 (2009).
24. McHaourab, H.S., Steed, P.R. & Kazmier, K. Toward the fourth dimension of membrane protein structure: insight into dynamics from spin-labeling EPR spectroscopy. *Structure* **19**, 1549–1561 (2011).
25. Freed, D.M., Horanyi, P.S., Wiener, M.C. & Cafiso, D.S. Conformational exchange in a membrane transport protein is altered in protein crystals. *Biophys. J.* **99**, 1604–1610 (2010).
26. Cross, T.A., Sharma, M., Yi, M. & Zhou, H.X. Influence of solubilizing environments on membrane protein structures. *Trends Biochem. Sci.* **36**, 117–125 (2011).
27. Hubbell, W.L., McHaourab, H.S., Altenbach, C. & Lietzow, M.A. Watching proteins move using site-directed spin labeling. *Structure* **4**, 779–783 (1996).
28. Jeschke, G. & Polyhach, Y. Distance measurements on spin-labelled biomacromolecules by pulsed electron paramagnetic resonance. *Phys. Chem. Chem. Phys.* **9**, 1895–1910 (2007).
29. Zhao, Y. *et al.* Single-molecule dynamics of gating in a neurotransmitter transporter homologue. *Nature* **465**, 188–193 (2010).
30. Claxton, D.P. *et al.* Ion/substrate-dependent conformational dynamics of a bacterial homolog of neurotransmitter:sodium symporters. *Nat. Struct. Mol. Biol.* **17**, 822–829 (2010).
31. Kniazeff, J. *et al.* An intracellular interaction network regulates conformational transitions in the dopamine transporter. *J. Biol. Chem.* **283**, 17691–17701 (2008).
32. Georgieva, E.R., Borbat, P.P., Ginter, C., Freed, J.H. & Boudker, O. Conformational ensemble of the sodium-coupled aspartate transporter. *Nat. Struct. Mol. Biol.* **20**, 215–221 (2013).
33. Hänelt, I., Wunnicke, D., Bordignon, E., Steinhoff, H.J. & Slotboom, D.J. Conformational heterogeneity of the aspartate transporter Glt_{Ph}. *Nat. Struct. Mol. Biol.* **20**, 210–214 (2013).
34. Polyhach, Y., Bordignon, E. & Jeschke, G. Rotamer libraries of spin labelled cysteines for protein studies. *Phys. Chem. Chem. Phys.* **13**, 2356–2366 (2011).
35. Polyhach, Y., Godt, A., Bauer, C. & Jeschke, G. Spin pair geometry revealed by high-field DEER in the presence of conformational distributions. *J. Magn. Reson.* **185**, 118–129 (2007).
36. Quick, M. *et al.* Binding of an octylglucoside detergent molecule in the second substrate (S2) site of LeuT establishes an inhibitor-bound conformation. *Proc. Natl. Acad. Sci. USA* **106**, 5563–5568 (2009).
37. Islam, S.M., Stein, R.A., McHaourab, H.S. & Roux, B. Structural refinement from restrained-ensemble simulations based on EPR/DEER data: application to T4 lysozyme. *J. Phys. Chem. B* **117**, 4740–4754 (2013).
38. Roux, B. & Islam, S.M. Restrained-ensemble molecular dynamics simulations based on distance histograms from double electron-electron resonance spectroscopy. *J. Phys. Chem. B* **117**, 4733–4739 (2013).
39. Zhao, Y. *et al.* Substrate-modulated gating dynamics in a Na^+-coupled neurotransmitter transporter homologue. *Nature* **474**, 109–113 (2011).

ONLINE METHODS

Mutagenesis, expression, purification and labeling of LeuT. All LeuT mutations were introduced into the recombinant LeuT construct containing an N-terminal decahistidine tag[21] by PCR-based site-directed mutagenesis and confirmed by DNA sequencing. Mutant LeuT was expressed in *Escherichia coli* BL21(DE3) as previously described[21]. LeuT was washed three times in 200 mM Tris-MES, pH 7.5, and 20% (v/v) glycerol to remove bound leucine and was subsequently extracted from native membranes with 40 mM (2% w/v) *n*-dodecyl-β-maltoside (β-DDM, Anatrace). LeuT was purified by Ni^{2+}-affinity chromatography and spin-labeled with 0.35 mM *S*-(2,2,5,5-tetramethyl-2,5-dihydro-1H-pyrrol-3-yl)methyl methanethiosulfonate spin label (MTSSL, Enzo Life Sciences) for 2 h at room temperature and 4 °C overnight. Spin-labeled LeuT was separated from free spin labels and aggregated protein by size-exclusion chromatography performed on a Shodex KW-803 column in a buffer consisting of 200 mM Tris-MES, 0.05% (w/v) β-DDM and 20% (v/v) glycerol at pH 7.2. LeuT was concentrated with Amicon Ultra columns (100 kDa, Millipore). For *n*-octyl-β-D-glucoside (β-OG, Anatrace) samples, Na^+ and excess leucine were added to Ni-affinity–purified LeuT, and the mixture was purified by size-exclusion chromatography in β-OG buffer (200 mM Tris-MES, pH 7.2, 200 mM NaCl, 1 μM leucine, 20% glycerol (v/v), and 40 mM (1.2% w/v) β-OG) and subsequently concentrated with Amicon Ultra columns (50 kDa, Millipore). Protein concentration was determined with an extinction coefficient of 1.91 cm^{-1} mg^{-1} at 280 nm for all mutants. All DEER samples were prepared in the 50–200 μM protein concentration range. A final concentration of glycerol of 30% (w/v) was used in all samples as a cryoprotectant. The Na^+-bound state was obtained by addition of 200 mM NaCl. The Na^+- and leucine-bound state was obtained by addition of four times molar excess of leucine to protein, in addition to 200 mM NaCl.

LeuT functional analysis. Equilibrium binding of [^{3}H]leucine (140 Ci/mmol; American Radiolabeled Chemicals) at the indicated concentrations and specific radioactivities was performed with the scintillation proximity assay (SPA)[40]. 0.8 pmol of unconcentrated purified and spin-labeled LeuT was bound to 250 μg copper-coated YSi-SPA beads (PerkinElmer) in 100 μL assay buffer (150 mM Tris-MES, pH 7.5, 50 mM NaCl, 1 mM TCEP, 20% (v/v) glycerol, and 0.1% (w/v) β-DDM) for 16 h at 4 °C before samples were measured in a Wallac photomultiplier tube MicroBeta microplate counter in the SPA mode. To determine the nonproximity background signal, samples were incubated in the presence of 800 mM imidazole, which competes with the histidine-tagged protein for binding to the copper-coated SPA beads. The nonproximity signal (in c.p.m.) was subtracted from the total c.p.m. (in the absence of imidazole) to obtain the specific c.p.m. Data points show the mean ± the s.e.m. of triplicate determinations normalized as a percentage of WT. Experiments were conducted with 100, 1,000 or 1,500 nM [^{3}H]leucine. Saturation binding curves were constructed for a subset of representative LeuT mutants by varying [^{3}H]leucine concentration between 10 nM and 5 μM and are normalized as a percentage of WT. Curves were fitted with the nonlinear curve-fit, one-site binding function in Origin 8 (OriginLab).

Transport assays of reconstituted LeuT variants were performed as described[21,40]. Briefly, purified LeuT variants were reconstituted at a 1:150 (w/w) ratio in preformed liposomes made of *E. coli* polar lipid extract (Avanti). 1 μM [^{3}H]alanine (49.4 Ci/mmol, Moravek) transport was measured for the indicated periods of time at 22 °C in assay buffer composed of 50 mM Tris-MES, pH 8.5, and 50 mM NaCl and was stopped by quenching with ice-cold 100 mM Kpi, pH 6.0, and 100 mM LiCl. This was followed by rapid filtration through 0.22-μm nitrocellulose filters (Millipore) and scintillation counting. C.p.m. were transformed into mol according to known amounts of [^{3}H]alanine.

DEER spectroscopy. Distance measurements were conducted on a Bruker 580 pulsed EPR spectrometer operating at Q-band frequency (33.9 GHz) with a standard four-pulse DEER sequence as previously described[41]. All DEER experiments were performed at 83 K. The frequency difference between pump and observed was typically 63 MHz. Dipolar evolution times were designed to allow identification of background slopes, when possible. Echo decays were shortened by 500 ns to remove the baseline step that results from overlap between pump and observed pulse, as previously described[42], background-corrected and fit with DEER Analysis 2011 (ref. 43) with Tikhonov regularization[44] to obtain distance distributions. Aggregated protein, resulting from concentration and validated by gel electrophoresis, appears in some samples as a nonspecific distribution peak near 50 Å. This peak shifts depending on the decay time of the echo, thus suggesting a broad distribution. This assignment was confirmed by reanalysis of the sample after DEER measurements by size-exclusion chromatography. Analysis of DEER data is shown in **Supplementary Figure 8**.

Rotamer simulation. Distance distributions for each mutant were simulated for LeuT crystal structures (PDB 2A65, PDB 3TT1 and PDB 3TT3) with the rotamer library–based prediction software MMM 2011 (refs. 34,35). Rotamer library calculations were conducted at 83 K.

Restrained ensemble simulations. The restrained ensemble (RE) simulation method[37,38] was used to model LeuT conformations with the DEER distance distribution data. The crystal structure of the Na^+- and leucine-bound occluded state (PDB 2A65)[6] was used to construct the initial geometry for the simulations. All simulations were carried out with CHARMM[45] modified to account for the DEER-distance histogram restraints via the RE simulation method. The all-atom CHARMM27 protein force field[46] with the CMAP corrections[47] was used. The dummy nitroxide spin label was parameterized and optimized previously from all-atom simulations of the MTSSL spin label to best match DEER data on several solvent-exposed sites in T4 lysozyme[37]. The EEF1 and IMM1 implicit membrane model[48,49] was used to mimic the bilayer membrane environment and was centered at Z = 0 with the membrane normal parallel to the Z axis. The EEF1 and IMM1 calculations were prepared with the implicit solvent modeler module in CHARMM-GUI (http://www.charmm-gui.org)[50]. The simulations were performed under NVT conditions at 300 K, and the Langevin[51] thermostat was used to control the temperature of the simulation box. A collision frequency, γ, of 1 ps^{-1} was used for the Langevin thermostat, and an integration time step of 1 fs was used. The nonbonded interactions were smoothly switched off from 7–11Å with a group-based cutoff. The multiple copies of the dummy spin labels were initially optimized with energy minimization and then replicated 25 times to yield a total of 625 distances between each spin-label pair for constructing the histograms. After a weakly restrained (10 kcal/mol·$Å^2$) 25-ps system equilibration, the RE simulation used r.m.s. deviation restraints (500 kcal/mol·$Å^2$) to maintain secondary structure in helical residues, positional harmonic restraints on residues 41–214 and 337–395 to maintain crystal-structure positions for static regions, and distance-distribution restraints to drive conformational change in dynamic regions. Distance-distribution data corresponding to apo, Na^+-bound, and Na^+- and leucine-bound intermediates were used for three different RE simulations. Each RE simulation was performed for 10 ns, which for each simulation was past the time required for r.m.s. deviation convergence to a constant value. An energy restraint was imposed via a large force constant (80,000 kcal/mol) in order to match the calculated spin-pair distance distributions with those of the experiment, with σ set to 1.7. The final structures thus obtained from the three RE simulations were then used for comparative analysis.

40. Quick, M. & Javitch, J.A. Monitoring the function of membrane transport proteins in detergent-solubilized form. *Proc. Natl. Acad. Sci. USA* **104**, 3603–3608 (2007).
41. Pannier, M., Veit, S., Godt, A., Jeschke, G. & Spiess, H.W. Dead-time free measurement of dipole-dipole interactions between electron spins. *J. Magn. Reson.* **142**, 331–340 (2000).
42. Jeschke, G. DEER distance measurements on proteins. *Annu. Rev. Phys. Chem.* **63**, 419–446 (2012).
43. Jeschke, G. *et al.* DeerAnalysis2006: a comprehensive software package for analyzing pulsed ELDOR data. *Appl. Magn. Reson.* **30**, 473–498 (2006).
44. Chiang, Y.W., Borbat, P.P. & Freed, J.H. The determination of pair distance distributions by pulsed ESR using Tikhonov regularization. *J. Magn. Reson.* **172**, 279–295 (2005).
45. Brooks, B.R. *et al.* CHARMM: The biomolecular simulation program. *J. Comput. Chem.* **30**, 1545–1614 (2009).
46. MacKerell, A.D. *et al.* All-atom empirical potential for molecular modeling and dynamics studies of proteins. *J. Phys. Chem. B* **102**, 3586–3616 (1998).
47. Mackerell, A.D., Feig, M. & Brooks, C.L. Extending the treatment of backbone energetics in protein force fields: limitations of gas-phase quantum mechanics in reproducing protein conformational distributions in molecular dynamics simulations. *J. Comput. Chem.* **25**, 1400–1415 (2004).
48. Lazaridis, T. Effective energy function for proteins in lipid membranes. *Proteins* **52**, 176–192 (2003).
49. Lazaridis, T. & Karplus, M. Effective energy function for proteins in solution. *Proteins* **35**, 133–152 (1999).
50. Jo, S., Kim, T., Iyer, V.G. & Im, W. CHARMM-GUI: a web-based graphical user interface for CHARMM. *J. Comput. Chem.* **29**, 1859–1865 (2008).
51. Adelman, S.A. & Doll, J.D. Generalized Langevin equation approach for atom-solid-surface scattering - general formulation for classical scattering off harmonic solids. *J. Chem. Phys.* **64**, 2375–2388 (1976).